Scalar Split WIMPs in the Future Direct Detection Experiments

Karim Ghorbani *

Physics Department, Faculty of Sciences, Arak University, Arak 38156-8-8349, Iran

Hossein Ghorbani†

Institute for Research in Fundamental Sciences (IPM)
School of Particles and Accelerators, P.O. Box 19395-5531, Tehran, Iran

Abstract

We consider a simple renormalizable dark matter model consisting of two real scalars with a mass splitting δ, interacting with the SM particles through the Higgs portal. We find a viable parameter space respecting all the bounds imposed by invisible Higgs decay experiments at the LHC, the direct detection experiments by XENON100 and LUX and the dark matter relic abundance provided by WMAP and Planck. Despite the singlet scalar dark matter model that is fragile against the future direct detection experiments, the scalar split model introduced here survives such forthcoming bounds. We emphasize on the role of the co-annihilation processes and the mixing effects in this feature. For $m_{\rm DM} \sim 63$ GeV in this model we can explain as well the observed gamma-ray excess in the analyses of the Fermi-LAT data at Galactic latitudes $2^\circ \leq |b| \leq 20^\circ$ and Galactic longitudes $|l| < 20^\circ$.

*kghorbani@ipm.ir
†pghorbani@ipm.ir

1 Introduction

Although there is no doubt on the existence of dark matter (DM) which is forming about 26 percent of the matter content of the Universe [1,2] (see e.g. reviews [3,4]), its fundamental interaction with ordinary matter of the Standard Model (SM) of particle physics is a tremendous mystery in physics today. There is however, a natural explanation for the present value of DM relic density in terms of the thermal freeze-out mechanism of weakly interacting massive particles (WIMPs). Exploiting the WIMP paradigm, a large number of theories beyond the SM is developed with a DM candidate as a WIMP, we name for instance supersymmetric models with R-parity , models with universal extra dimensions, as well as models with minimal extension of the SM which is of our interest in this article [5–12].

All these models can receive stringent constraints on the DM annihilation cross section from Planck [1] and WMAP [2], precise measurements of the DM relic density, and on the WIMP-nucleon scattering cross section from dark matter experiments such as LUX [13] and XENON100 [14]. Moreover, in the case of DM production in particle collider experiments, there are measurements such as invisible Higgs decay and missing energy-momentum that can put further restrictions on the model parameter space [15–18].

The new bounds by the coming direct detection experiments such as XENON1T which is going to start data collection already in this autumn, will certainly exclude many of the current WIMP models. The popular singlet scalar dark matter model as the most minimal extension of the SM has been investigated elaborately from different points of view in the literature (see for instance [5,6,19,20]). Although this model is fairly successful in various aspects, it is quite in danger to be excluded for a wide range of DM mass due to the direct detection experiments that will put stringent bounds in the near future [21]. If the direct detection experiments are taken seriously and one is still interested in the scalar extension of the SM, the next minimal model that comes to mind is the two real scalar extension dubbed here under the name of *scalar split WIMPs*. We show in this paper that scalar split model is as good as the singlet scalar model with drastically improved features in the direct detection part.

On the other hand, in the light of the recent confirmed observation of the Fermi-LAT extended gamma ray excess, many investigations have directed towards possible explanation of the gamma excess. Assuming that the galactic gamma excess produced as a result of DM annihilation in the galactic center, it is then found in a number of models that DM annihilation cross section of order $\sim 10^{-26}$ cm^{3}s^{-1} with DM mass in the range $30 - 50$ GeV can explain the excess, see as examples [22–49], and see [50–54] for scenarios with lighter DM. Later it was found in [55–57] that DM mass of $\sim 35 - 165$ GeV decaying into b quark pair and DM mass large enough to decay into W^+W^-, ZZ, hh, $\bar{t}t$ pairs can be fitted satisfactorily to the Fermi-LAT data.

In this paper we consider a minimal extension of the SM with two additional real scalars denoted by S_1 and S_2, which are SM gauge singlets and interact with the SM particles via a Higgs portal respecting the $\mathbb{Z}_2$ symmetry under which the new scalars are odd and all the SM particles are even. This model suggests two scalar WIMPs with a mass splitting δ where only the lighter component is stable and the heaver one

is an unstable state [8]. The viable parameter space constrained by the limits from the observed DM relic abundance, direct detection bounds as well as invisible Higgs decay width is studied in this work. We also show that it is possible to find regions in the viable parameter space which can explain the galactic gamma ray excess observed by Fermi-LAT.

The rest of the paper has the following structure. In section 2 the scalar split model is introduced and the relevant free parameters are discussed. In section 3 we discuss how to calculate the relic density using the DM annihilation cross sections. Section 4 is devoted to calculations on the Higgs decay to two WIMPs and invisible Higgs decay width is provided in terms of the mass range of the DM candidate. Moreover, the viable parameter space constrained by the DM relic density observation as well as invisible Higgs decay width are studied. Elastic scattering cross section of DM-nucleon is computed as a function of DM mass in section 5, taking into account the limits from relic density observation and direct detection experiments. In section 6 we find how it is possible to explain the inner galactic gamma ray excess within the constrained model parameters. We finish in section 7 with the conclusion.

2 Scalar Split WIMPs

We consider a renormalizable extension to the SM with two new real scalar fields denoted by S_1 and S_2. These new fields may have small mass splitting and transform under $\mathbb{Z}_2$ symmetry as $S_i \to -S_i$. The full Lagrangian consists of

$$\mathcal{L} = \mathcal{L}_{\rm SM} + \mathcal{L}_{\rm DM} + \mathcal{L}_{\rm int}\,. \tag{1}$$

The Lagrangian $\mathcal{L}_{\rm DM}$ incorporates only the WIMPs particles as

$$\mathcal{L}_{\rm DM} = \frac{1}{2}(\partial_\mu S_1)^2 + \frac{1}{2}(\partial_\mu S_2)^2 - \frac{m_1^2}{2}S_1^2 - \frac{m_2^2}{2}S_2^2 - \frac{\lambda_3}{4}S_1^4 - \frac{\lambda_4}{4}S_2^4\,. \tag{2}$$

We could in principle have the interaction term $\lambda_s S_1^2 S_2^2$ in the lagrangian (2). We will turn to this point later in this section.

In addition, respecting the $\mathbb{Z}_2$ symmetry, WIMPs interaction with the SM particles are considered through a Higgs portal such that

$$\mathcal{L}_{\rm int}(S_1, S_2, H) = \lambda_1 S_1^2 H^\dagger H + \lambda_2 S_2^2 H^\dagger H + \lambda_{12} S_1 S_2 H^\dagger H\,. \tag{3}$$

The SM-Higgs potential is also given by

$$V_H = \mu_H^2 H^\dagger H + \lambda_H (H^\dagger H)^2\,. \tag{4}$$

The Higgs field is a SM $SU(2)_L$ scalar doublet which develops a non-zero vacuum expectation value (vev) which results in the electroweak spontaneous symmetry breaking. We then parameterize H as

$$H = \frac{1}{\sqrt{2}}\begin{pmatrix} 0 \\ v+h \end{pmatrix}\,, \tag{5}$$

where $v = 246$ GeV.

We can choose a basis in which $\langle S_1 \rangle = \langle S_2 \rangle = 0$. The minimization conditions of the total potential are

$$\frac{\partial V}{\partial H}\Big|_{\langle H \rangle = v/\sqrt{2}} = \frac{\partial V}{\partial S_1}\Big|_{\langle S_1 \rangle = 0} = \frac{\partial V}{\partial S_2}\Big|_{\langle S_2 \rangle = 0} = 0\,. \tag{6}$$

These conditions provide us with some relations between the parameters. We work them out and identify the entries of the mass matrix. From condition $\frac{\partial V}{\partial H}\big|_{\langle H \rangle} = 0$ we get the relation

$$\mu_H^2 = -\lambda_H v^2\,. \tag{7}$$

From the other two minimization conditions we get no more relation. We also get the following results for the entries of the mass matrix

$$m_{S_1}^2 = \frac{\partial^2 V}{\partial S_1^2} = m_1^2 + \lambda_1 v^2\,, \quad m_{S_2}^2 = \frac{\partial^2 V}{\partial S_2^2} = m_2^2 + \lambda_2 v^2\,, \tag{8}$$

and

$$m_{S_1,S_2}^2 = \frac{\partial^2 V}{\partial S_1 \partial S_2} = \frac{1}{2}\lambda_{12} v^2\,. \tag{9}$$

We then indicate the two fields H_1 and H_2 as the mass eigenstates by introducing the mass mixing angle θ

$$\begin{aligned} H_1 &= \sin\theta\ S_1 + \cos\theta\ S_2\,, \\ H_2 &= \cos\theta\ S_1 - \sin\theta\ S_2\,, \end{aligned} \tag{10}$$

where,

$$\tan\theta = \frac{y}{1+\sqrt{1+y^2}}\,, \quad \text{with} \quad y = \frac{2m_{S_1,S_2}^2}{m_{S_2}^2 - m_{S_1}^2}\,. \tag{11}$$

The two neutral scalars H_1 and H_2 have the corresponding mass eigenvalues as

$$m_{H_1,H_2}^2 = \frac{m_{S_1}^2 + m_{S_2}^2}{2} \pm \frac{m_{S_2}^2 - m_{S_1}^2}{2}\sqrt{1+y^2}\,. \tag{12}$$

We assume that $m_{H_1} > m_{H_2}$ and therefore H_2 is the stable DM candidate. It is then possible to obtain relations for m_1 and m_2 in terms of physical masses and couplings

$$\begin{aligned} m_1^2 &= m_{H_1}^2 \sin^2\theta + m_{H_2}^2 \cos^2\theta - \lambda_1 v^2\,, \\ m_2^2 &= m_{H_1}^2 \cos^2\theta + m_{H_2}^2 \sin^2\theta - \lambda_2 v^2\,. \end{aligned} \tag{13}$$

Moreover, from eq. (9), eq. (11) and eq. (12) we can express the coupling λ_{12} in terms of the masses m_{H_1} and m_{H_2} and the mixing angle θ,

$$\lambda_{12} = \frac{2}{v^2}(m_{H_1}^2 - m_{H_2}^2)\sin 2\theta\,. \tag{14}$$

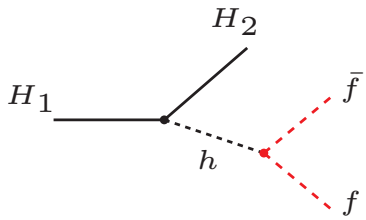

Figure 1: Three body decay of the scalar H_1 into the scalar DM and a fermion pair.

We now turn to the point we made after equation (2). If we rewrite the lagrangian (2) in the basis of mass eigenstates H_1 and H_2, then it includes a term for interacting DM with its parter as $6\sin^2\theta\cos^2\theta(\lambda_3+\lambda_4)H_1^2H_2^2$. Taking $m_{H_1} > m_{H_2}$ it means that the co-annihilation process $H_2H_2 \to H_1H_1$ kinematically is not allowed. Adding the $\lambda_s S_1^2 S_2^2$ term do not introduce any new interactions in the lagrangian after going to the mass eigenstate basis, although it modifies the strengths by the new coupling λ_s. For instance, the term above changes as $\left(6\sin^2\theta\cos^2\theta(\lambda_3+\lambda_4-12\lambda_s)+6\lambda_s\right)H_1^2H_2^2$, which again do not contribute in the relic density computation. Therefore, the term $S_1^2S_2^2$ merely enlarges the dimension of the parameter space by one. To stay in the most minimal scenario possible we assume that $\lambda_s = 0$ in this paper.

We therefore can take in the present model seven independent parameters as m_{H_1}, m_{H_2}, λ_1, λ_2, λ_3, λ_4 and θ, while the coupling λ_{12} is then fixed by the relations in eq. (11) and eq. (14). The vacuum stability of the total potential restricts the model parameters. In this regards, we find at tree level the bounds

$$\begin{aligned} m_1^2 + m_2^2 + (\lambda_1+\lambda_2)v^2 > 0\,, \\ m_1^2m_2^2 + (m_1^2\lambda_1 + m_2^2\lambda_2)v^2 + \lambda_1\lambda_2 v^4 > \lambda_{12}^2 v^4\,. \end{aligned} \tag{15}$$

In addition, the perturbativity of the model requires the upper bounds on the couplings, $|\lambda_i| < 4\pi$.

When the small mass splitting is the case then the heavy component WIMP can decay into an off-shell Higgs and the light partner as $H_1 \to H_2 h$ where h itself decays successively into a fermion pair as $h \to \bar{f}f$. The Feynman diagram for the decay is shown in Fig. 1.

It is necessary to have an estimate on the life time of the heavy component over the restricted parameter space to know whether or not it has any contribution on the DM relic abundance. We provide here the formula of the double differential partial decay width for $H_1(k) \to H_2(p_3)\ \bar{f}(p_1)\ f(p_2)$

$$\frac{d^2\Gamma}{dt\ du} = \frac{3m_f^2[(\lambda_1-\lambda_2)\sin 2\theta + \lambda_{12}\cos 2\theta\ ]^2}{128\pi^3 m_{H_1}^3}\Big[\frac{t+m_h^2-m_{H_2}^2-4m_f^2}{(t-m_h^2)^2+\Gamma_h^2 m_h^2}\Big]\,, \tag{16}$$

where the mandelstam variables are $t = (p_1+p_2)^2$ and $u = (p_2+p_3)^2$.

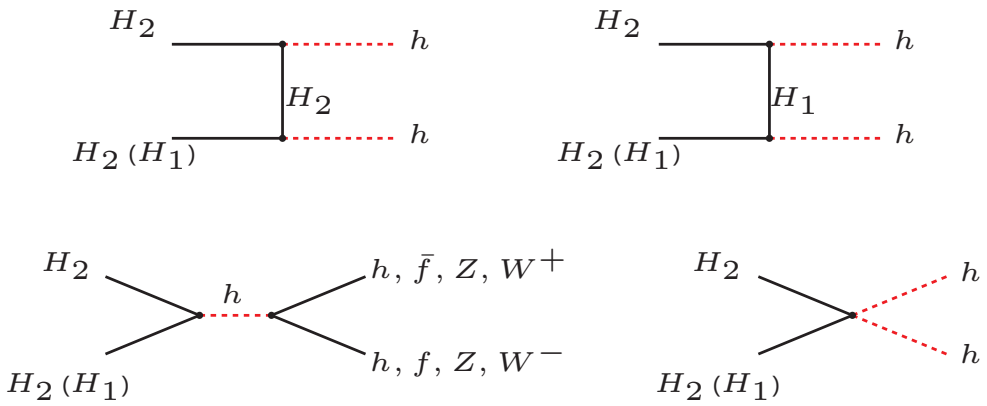

Figure 2: The Feynman diagrams for the DM (co)-annihilation into SM final states. Diagrams with more than two particles in the final state are not shown.

3 Dark Matter Relic Abundance

Assuming that DM particles have been in thermal equilibrium in the early Universe, the present density of DM depends somehow on the so-called freeze-out temperature, T_f, the epoch in which dark particles become non-relativistic and go out of the equilibrium. At freeze-out temperature the annihilation rate of DM falls off below the Hubble expansion rate. On the other side, due to the low budget of the kinetic energy, the DM production reactions get suppressed. The relic density of DM is computed by solving the Boltzmann equation(s) for the time evolution of DM number density, $n_{\rm DM}$. In the model under consideration, there are two new scalars beside the SM particles that their number density evolutions are relevant in order to obtain the DM relic abundance. We assume that H_2 is the lighter component and thus is stable. We therefore consider H_2 as our DM candidate with mass m_{H_2} that $m_{H_1} > m_{H_2}$. So the heavier scalar H_1 can undergo the decay $H_1 \to H_2 + \text{SM}$.

Annihilation reactions are one type of processes that change the number density (n_1 and n_2) of our species here. The possible annihilations of H_1 and H_2 to SM particles are depicted in Fig. 2. As it is evident from the Feynman diagrams, annihilation reactions into SM fermion pairs, W^+W^- and ZZ occur via s-channel while annihilation into SM-Higgs pair is possible through s-, t- and u-channel. An annihilation process in which DM particle annihilates together with H_1 is the so-called *co-annihilation* reaction. Another type of reaction that changes the number density is the decay process of the heavier component, i.e., H_1. In principle, the abundance of H_1 and H_2 are determined by solving two coupled Boltzmann equations. The two Boltzmann equations can be written in a single Boltzmann equation with an effective (co-)annihilation cross section [58–60],

$$\frac{dn}{dt} = -3Hn - \langle \sigma_{\rm eff}\, v \rangle \left(n^2 - n_{eq}^2 \right) \ , \tag{17}$$

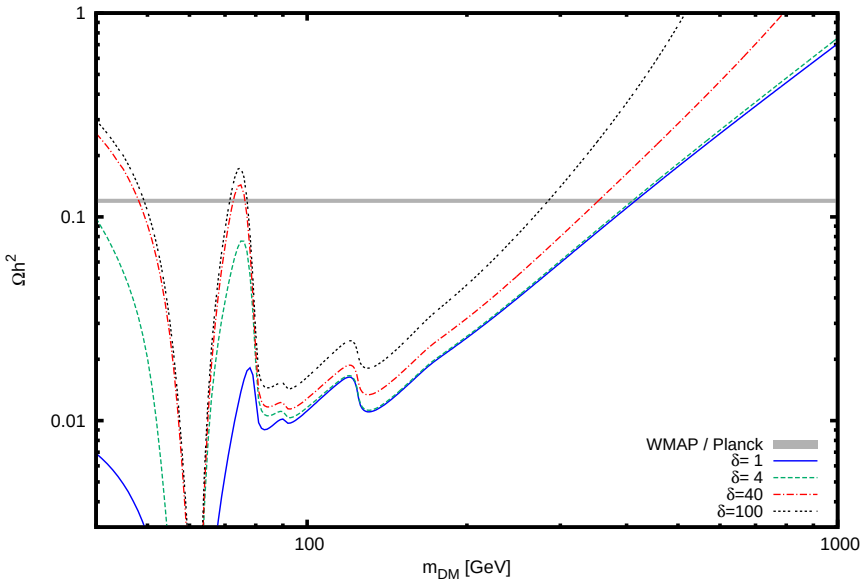

Figure 3: The dependency of the relic density on the mass splitting δ for a wide range of DM mass.

where $n \equiv n_{H_1} + n_{H_2}$ and

$$\sigma_{\text{eff}} = \frac{1}{g_{\text{eff}}} \left(\sigma_{22} + \sigma_{11} \left(1 + \frac{\delta}{m_{H_2}}\right)^3 e^{-2\delta/T} + 2\sigma_{12} \left(1 + \frac{\delta}{m_{H_2}}\right)^{3/2} e^{-\delta/T} \right) , \qquad (18)$$

where σ_{22}, σ_{11} and σ_{12} stand for (co-)annihilation processes $H_2 H_2 \to \text{SM}\,\text{SM}$, $H_1 H_1 \to \text{SM}\,\text{SM}$ and $H_2 H_1 \to \text{SM}\,\text{SM}$ respectively with $g_{\text{eff}} = 1 + \left(1 + \frac{\delta}{m_{H_2}}\right)^{3/2} e^{-\delta/T}$.

The expression $\langle \sigma_{\text{eff}}\, v \rangle$ indicates thermal average over effective annihilation cross section $\times$ relative velocity at temperature T. In appendix A we present the formulas for annihilation cross sections of dark matter candidate in four possible channels. To confirm our analytical formula we employ the program CalcHEP [61] which in turn requires implementation of our model into the program LanHEP [62]. To perform the analysis for the DM relic abundance we need to solve numerically the Boltzmann equation. To this end, we utilize the program MicrOMEGAs [63] for our model.

As explained earlier we have two choices for a set of independent parameters we would like to place the constraints on. Notice that the couplings λ_3 and λ_4 do not show up in DM annihilation cross sections at the tree level, however these couplings appear through the strength of the vertex $H_1^2 H_2^2$. We fix the two couplings as $\lambda_3 = \lambda_4 = 0$. Therefore, one possibility is choosing the set of parameters $\{m_{H1}, m_{H_2}, \lambda_1, \lambda_2, \lambda_{12}\}$ and the other option is the set $\{m_{H_1}, m_{H_2}, \lambda_1, \lambda_2, \theta\}$. In our analysis we choose the second set and apply the relation in eq. (14) to obtain the coupling λ_{12} by fixing the mixing angle θ.

Let us define the mass splitting as $\delta \equiv \Delta m_{12} = m_{H_1} - m_{H_2}$. Taking into account the co-annihilation processes, we check numerically the dependency of the relic den-

sity on the mass splitting δ. For a point in the parameter space with $\lambda_1 = 0.56$, $\lambda_2 = 0.33$ and $\sin\theta = 0.1$, the results are compared in Fig. 3 for $\delta = 1$ GeV, 4 GeV, 40 GeV and 100 GeV. Since the co-annihilation effects are larger for smaller value of δ, for the present model, it is evident from Fig .3 that the relic density is reduced by the co-annihilation effects.

4 Invisible Higgs Decay

The DM candidate in the scalar split model interacts with the SM particles via SM-Higgs mediator. It also opens up the possibility for the 125 GeV Higgs to decay into the new scalars. Constraints on the model parameters are placed by requiring the invisible Higgs decay to be consistent with the Large Hadron Collider (LHC) measurements. The total decay width of 125 GeV Higgs decaying into SM particles is ~ 4.1 MeV [64] which get enhanced by three invisible decay width of the SM-Higgs, $h \to H_1 H_1$, $h \to H_1 H_2$ and $h \to H_2 H_2$. Given an experimental upper limit for the invisible branching ratio for the Higgs boson as $\Gamma_{\rm inv}/(\Gamma_{\rm inv} + \Gamma_{\rm v}) \sim 0.35$ [18] we put a bound on the total invisible decay width as $\Gamma_{\rm inv}^{\rm total} < 2.15$ MeV. On the other hand, the total invisible decay width in this model is saturated by three possible decays of the Higgs:

$$\Gamma_{\rm inv}^{11}(h \to H_1 H_1) = \frac{v^2(\lambda_1 \sin^2\theta + \lambda_2 \cos^2\theta + \lambda_{12} \sin\theta\cos\theta)^2}{8\pi m_h}(1 - \frac{4m_{H_1}^2}{m_h^2})^{1/2}\,, \quad (19)$$

$$\Gamma_{\rm inv}^{22}(h \to H_2 H_2) = \frac{v^2(\lambda_1 \cos^2\theta + \lambda_2 \sin^2\theta - \lambda_{12} \sin\theta\cos\theta)^2}{8\pi m_h}(1 - \frac{4m_{H_2}^2}{m_h^2})^{1/2}\,, \quad (20)$$

and

$$\Gamma_{\rm inv}^{12}(h \to H_1 H_2) = \frac{v^2[(\lambda_1 - \lambda_2)\sin 2\theta + \lambda_{12}\cos 2\theta]^2}{8\pi m_h^3} \times [m_h^2 - (m_{H_1}^2 + m_{H_2}^2)^2]^{1/2}[m_h^2 - (m_{H_1}^2 - m_{H_2}^2)^2]^{1/2}\,. \quad (21)$$

The invisible Higgs decay width depends on DM mass m_{H_2} and δ as the following:

$$\begin{aligned}
\Gamma_{\rm inv}^{\rm total} &= \Gamma_{\rm inv}^{22} && \text{when} \quad \frac{m_h}{2} - \frac{\delta}{2} < m_{H_2} < \frac{m_h}{2}\,,\\
\Gamma_{\rm inv}^{\rm total} &= \Gamma_{\rm inv}^{22} + \Gamma_{\rm inv}^{12} && \text{when} \quad \frac{m_h}{2} - \delta < m_{H_2} < \frac{m_h}{2} - \frac{\delta}{2}\,,\\
\Gamma_{\rm inv}^{\rm total} &= \Gamma_{\rm inv}^{22} + \Gamma_{\rm inv}^{12} + \Gamma_{\rm inv}^{11} && \text{when} \quad m_{H_2} < \frac{m_h}{2} - \delta\,.
\end{aligned} \quad (22)$$

Let us now begin with our probe over the parameter space of the model. To proceed we put together the constraints imposed on the parameter space from relic density analysis and the invisible Higgs decay width. This has been done for two values of the mass splitting $\delta = 1$ GeV and $\delta = 100$ GeV in order to investigate the role of this parameter on the viable space and confronting that with the singlet scalar dark matter case.

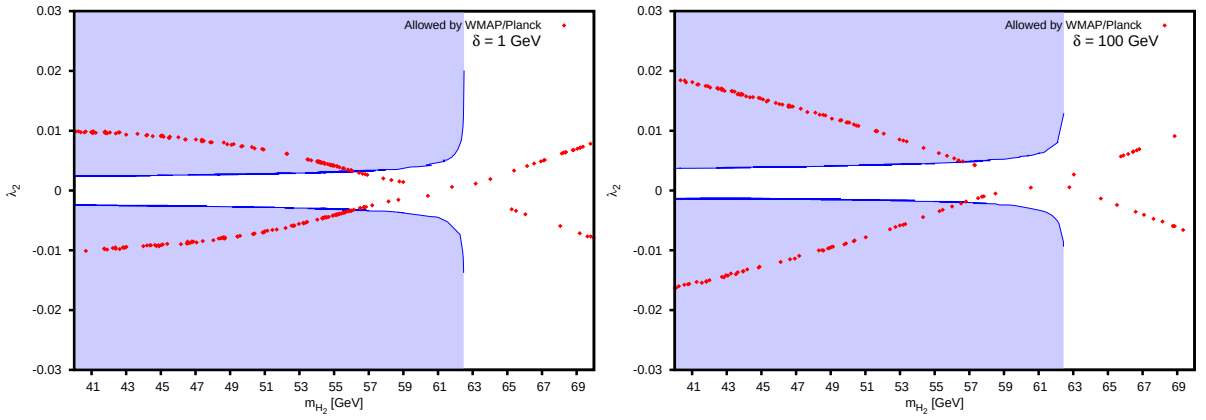

Figure 4: Shown are the allowed DM mass in the viable parameter space respecting the relic density and invisible Higgs decay width constraints for *left*) $\delta = 1$ GeV *right*) $\delta = 100$ GeV.

We have generated random values for DM mass with 40 GeV $< m_{H_2} < m_h/2$, $-1 < \lambda_1 < 1$, and taking $\lambda_2 = \lambda_1/5$ and $\sin\theta = 0.1$. Using the combined results from WMAP and Planck for the present DM relic density, the results exhibited in Fig. 4 show the viable parameter space for different values of the mass splitting parameter δ. The region colored in blue is excluded by the invisible Higgs decay width. There are some comments in order for the Fig. 4:

First, for DM mass below $m_h/2$, only DM annihilation into fermions mediated via SM-Higgs are potentially allowed processes, thus one expects enhancement on the cross section near the SM-Higgs mass resonance. It is evident from Fig. 4 that the resonance occurs around DM mass $m_{H_2} \sim m_h/2 \sim 62$ GeV where the coupling λ_2 (as well as the annihilation cross section) takes its smallest value, while λ_2 grows up for DM masses smaller or greater than the resonance mass 62 GeV. Moreover, it is seen that for both mass splittings $\delta = 1$ GeV and $\delta = 100$ GeV all DM masses smaller than $m_{H_2} \sim 56$ GeV are excluded. Finally, the range of the allowed DM mass in the scalar split model is almost the same as that of the single scalar dark matter model where $m_{\rm DM} < 55$ GeV is excluded by the LHC bounds on the invisible Higgs decay width [21].

5 Direct Detection

Direct detection experiments are designed to study the unknown nature of DM interaction with ordinary matter. In these experiments the attempt is to measure the enticing event rate for the DM scattering off the target nuclei in the detector. Although the present results from DM experiments such as LUX [13] and XENON100 [14] show no evidence for DM interactions, they offer an impressive upper bound on the spin-independent DM-nucleon elastic scattering cross section. We will apply these findings in the following to constrain further the parameter space of our model which is already restricted by the limits from WMAP and Planck. To this end, we need to

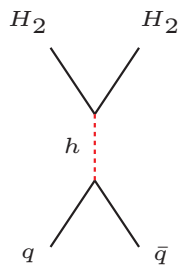

Figure 5: The relevant Feynman diagram for the WIMP-nucleon elastic scattering.

calculate the elastic scattering of WIMP-nucleon. In the present particular model the interaction of DM with nucleon occurs through a fundamental interaction of DM with quark which is mediated by the SM-Higgs, where the relevant Feynman diagram is depicted in Fig. 5. The effective Lagrangian responsible for the DM-quark interaction is,

$$\mathcal{L}_{\text{eff}} = \alpha_q H_2 H_2 \; \bar{q} q \,, \tag{23}$$

where, the coupling α_q is given by

$$\alpha_q = \frac{m_q}{m_h^2}(\lambda_1 \cos^2\theta + \lambda_2 \sin^2\theta - \lambda_{12} \sin\theta \cos\theta). \tag{24}$$

To find the elastic scattering cross section we can invoke the assumption that in the limit of vanishing momentum transfer it is possible to replace the nucleonic matrix element including quark current with that containing nucleon current up to some proportionality factor [65–68], see also [69]. We arrive at the final result for the spin-independent (SI) cross section of DM-nucleon as

$$\sigma_{\text{SI}}^{\text{N}} = \frac{\alpha_N^2 \mu_N^2}{\pi m_{\text{DM}}^2} \,, \tag{25}$$

where μ_N is the reduced mass of the DM-nucleon system and the factor α_N depends on the scalar couplings f_{Tq}^N and f_{Tg}^N as

$$\alpha_N = m_N \sum_{q=u,d,s} f_{Tq}^N \frac{\alpha_q}{m_q} + \frac{2}{27} f_{Tg}^N \sum_{q=c,b,t} \frac{\alpha_q}{m_q} \,. \tag{26}$$

In our numerical calculations we use the following values for the scalar couplings

$$f_u^p = 0.0153, \qquad f_d^p = 0.0191, \qquad f_s^p = 0.0447 \,. \tag{27}$$

We compute the elastic scattering cross section for about 10^6 points in the parameter space by random generation of the relevant parameters with $-1 < \lambda_1 < 1$, $-1 < \lambda_2 < 1$, 40 GeV $< m_{\text{DM}} <$ 3 TeV and $\sin\theta = 0.1$. We report on our numerical results for the elastic scattering cross section of DM-proton in Fig. 6 and Fig. 7, considering four different mass splittings in the model, namely $\delta = 1, 10, 40, 100$ GeV. We

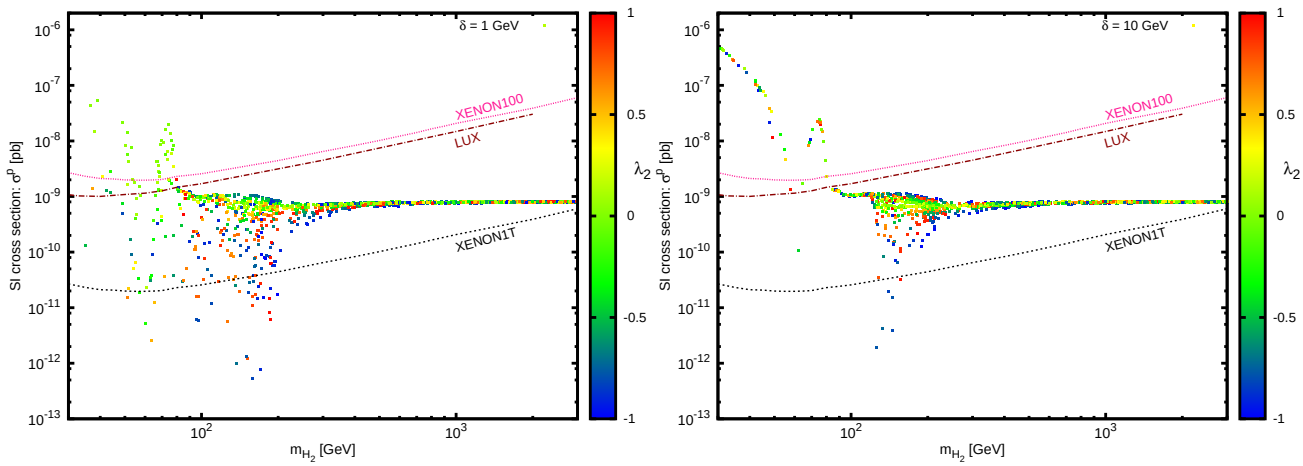

Figure 6: Spin-independent DM-nucleon elastic scattering cross section are shown as a function of the DM mass and comparison has made with the latest results from LUX and XENON100 experiments and the future experiment XENON1T. In the left panel the mass splitting is $\delta = 1$ GeV and in the right panel $\delta = 10$ GeV. The vertical color spectrum indicates the size of λ_2. We have chosen for the couplings as $-1 < \lambda_1 < 1$ and $-1 < \lambda_2 < 1$.

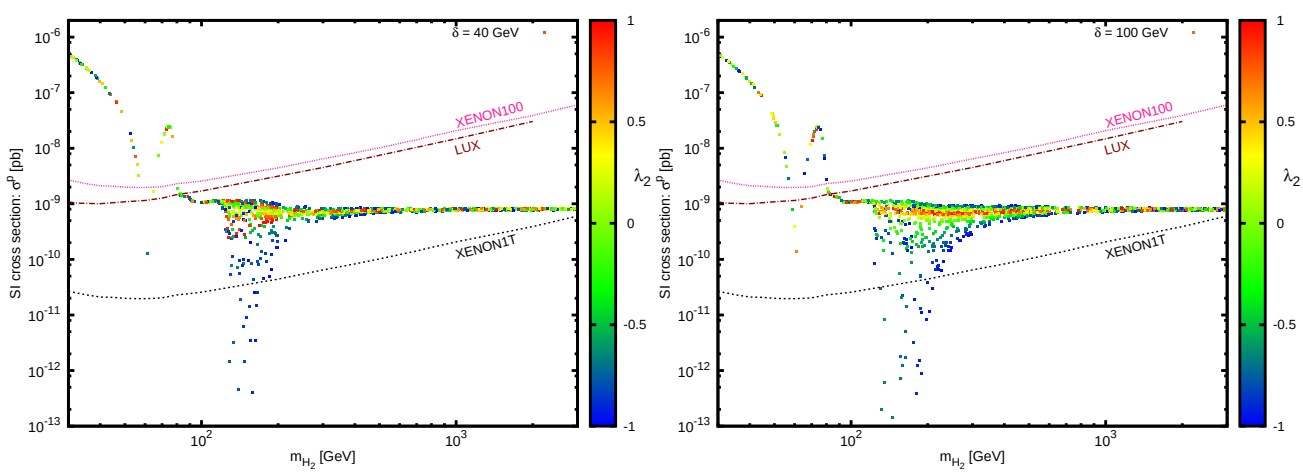

Figure 7: The same as in Fig. 6 with the left panel for the mass splitting $\delta = 40$ GeV and the right panel for $\delta = 100$ GeV.

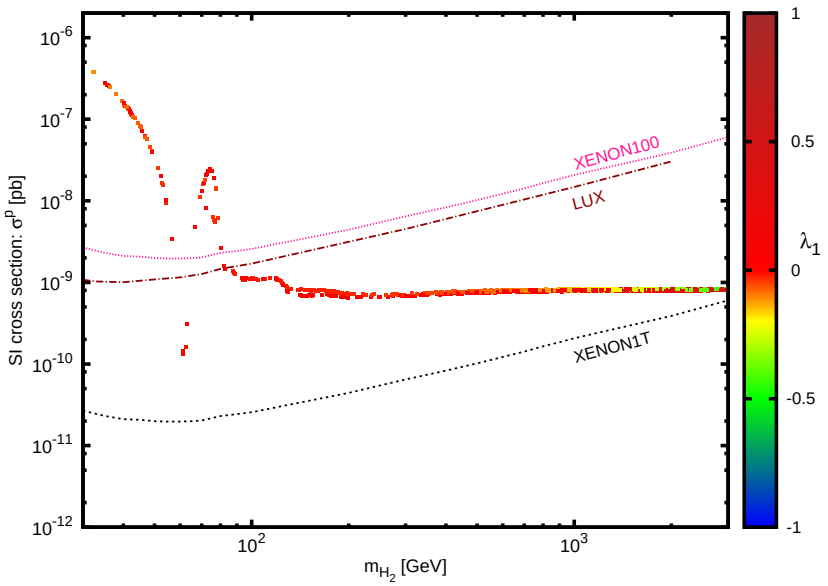

Figure 8: The elastic scattering cross section with $\sin\theta = 0$ for the parameter space bounded by the present Universe DM relic density.

have exploited the viable parameter space fulfilling already the relic density bound to obtain numerically the elastic scattering cross sections for a wide range of DM mass. These results have been plotted against the experimental bounds provided by LUX and XENON100 and the estimated bound for the future XENON1T.

In all plots it can be seen easily that the cross section falls off suddenly at the Higgs mass resonance region as pointed out before in section 4. It is for the resonance mass, i.e., around 62 GeV and for $m_{\rm DM} \gtrsim 4$ TeV that the singlet scalar model [21] can evade the future direct detection bounds. The success for the scalar split model is that it not only can evade the LUX and the XENON100 constraints but there are many DM candidates for which the values of the elastic scattering cross sections go even much below the future direct detection experiments such as XENON1T for a quite wide range of DM mass. This feature is true for all mass splittings δ. However, the viable parameter space is slightly sensitive to the mass splitting as seen in Figs. 6 and 7. When δ is small, i.e., when DM scalar and its partner in the model have more or less the same mass, the viable DM mass can be in the range $\sim 50 - 200$ GeV for $\delta = 1$ GeV if we consider the constraints imposed by XENON1T. With increasing the mass splitting δ, the viable DM mass is limited to values in the range $\sim 125 - 200$ GeV. It seems therefore that for small enough δ the parameter space is greater than that with much bigger δ. Looking at Fig. 3, note that for the viable space, i.e., for $m_{\rm DM} \sim 125 - 200$ GeV, the relic density does not change considerably going from $\delta = 1$ GeV to $\delta = 100$ GeV. On the other hand, the value of the splitting mass δ can make a big change in the relic density for $m_{\rm DM} \lesssim 60$ GeV and $m_{\rm DM} \gtrsim 400$ GeV.

We claim that the improvement in the spin-independent DM-nucleon scattering cross section for the present scalar split model of DM stems from two distinct effects.

One is the contribution of the co-annihilation processes and the other one is what we call it *mixing effect*. These two effects do not exist in the singlet scalar DM model. To clarify this statement, we repeat the computation for the DM-nucleon scattering cross section for $\sin\theta = 0$ where the contribution from the co-annihilation processes in the relic density and the mixing effect are both absent. The results for $\sigma_{\rm SI}$ that respect the relic density bound is plotted in Fig. 8. This figure actually accounts for the similar results presented in [21] for the singlet scalar DM model. It is evident from Fig. 8 that the feature in Fig. 6 and 7 disappears in the case $\sin\theta = 0$. There is a simple explanation why the new feature is not possible in the single scalar model. The reason hinges in the fact that in this case, both the annihilation cross section and the DM-nucleon scattering cross section are proportional to one common parameter, λ_1, as can be seen from the formulas provided in the appendix A. So that it is not possible to get simultaneously a quite small value for the DM-nucleon scattering cross section and a large enough annihilation cross section suitable for predicting the observed relic density.

The question we would like to address here is that why the new feature for large δ starts appearing in the region with $m_{\rm DM} \gtrsim 125$ GeV when $\theta \neq 0$. We know that for $m_{\rm DM} < 125$ GeV, only the processes, $H_2H_2 \to \bar{f}f, W^+W^-, ZZ$ contribute to the total annihilation cross section. Looking at the relevant formulas given in the appendix A, we find out that both the annihilation cross section and DM-nucleon scattering cross section are proportional to one common parameter, β, where $\beta = \lambda_1 \cos^2\theta + \lambda_2 \sin^2\theta - \lambda_{12} \sin\theta\cos\theta$. Therefore, we can apply the same line of reasoning as we did in the singlet model to understand why in the region with $m_{\rm DM} < 125$ GeV we see the same prediction as the one in the singlet model. Of course, for small mass splitting, i.e., $\delta = 1$ GeV the co-annihilation effects are sizable such that for $m_{\rm DM} < 125$ GeV, the spilt scalar model and singlet model show different predictions for the DM-nucleon scattering cross section. Now, when $m_{\rm DM}$ gets values larger than 125 GeV, the process $H_2H_2 \to hh$ starts dominating the total annihilation cross section. Here we expect the mixing effects show up. In this region it is totally possible to find quite small values for β and hence small DM-nucleon scattering cross section. At the same time having large values for α results in large enough annihilation cross section, where $\alpha = (\lambda_1 - \lambda_2)\sin 2\theta + \lambda_{12}\cos 2\theta$. To see this point, we need to look at eq. (32) in the appendix A. We see that even when β is small, the annihilation cross section can be large enough since α is not necessarily small and terms involving α will dominate the annihilation cross section. We have justified this latter claim in our numerical computations. When DM mass is larger than ~ 188 GeV such that the process $H_2H_2 \to hhh$ becomes kinematically possible, the aforementioned mixing effects discussed above are plausible, however, their strength would depend on the size of the couplings λ_1, λ_2 and δ. Heavier DM with mass $m_{\rm DM} \gtrsim 250$ GeV will open the new channel $H_2H_2 \to hhhh$ and we can see its small effects in Fig 6 and Fig 7.

We redo our computations with couplings in the range $-5 < \lambda_1 < 5$ and $-5 < \lambda_2 < 5$ for $\delta = 1, 10, 40, 100$ GeV. Our results given in Fig. 9 for $\delta = 1, 10$ GeV indicate that for larger values of the couplings λ_1 and λ_2, DM candidates which can evade XENON1T constraints are extended to masses up to ~ 1000 GeV. The DM candidates are extended to masses up to ~ 500 GeV in case $\delta = 40, 100$ GeV, as

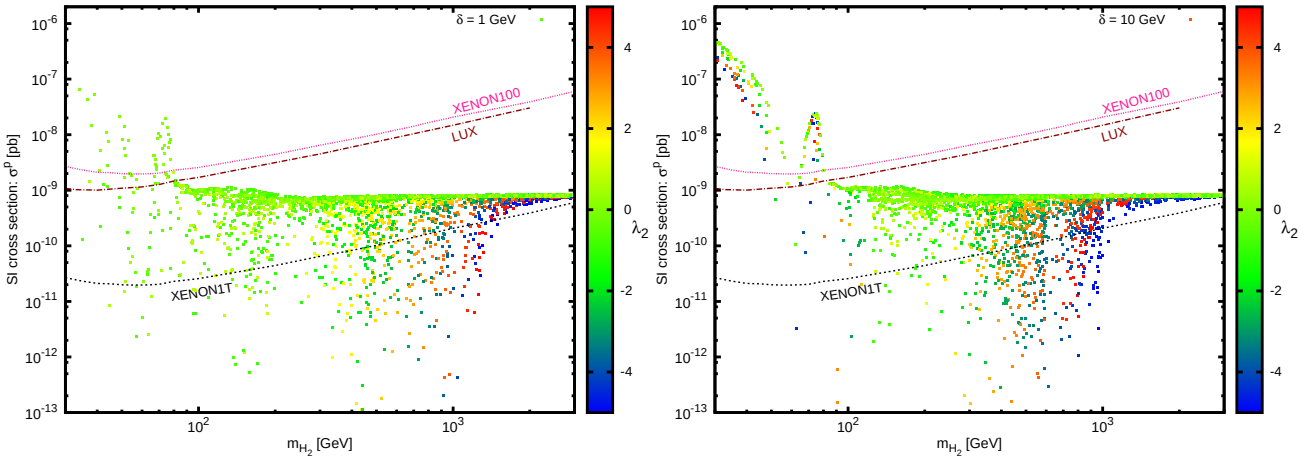

Figure 9: The same as in Fig. 6 with $-5 < \lambda_1 < 5$ and $-5 < \lambda_2 < 5$.

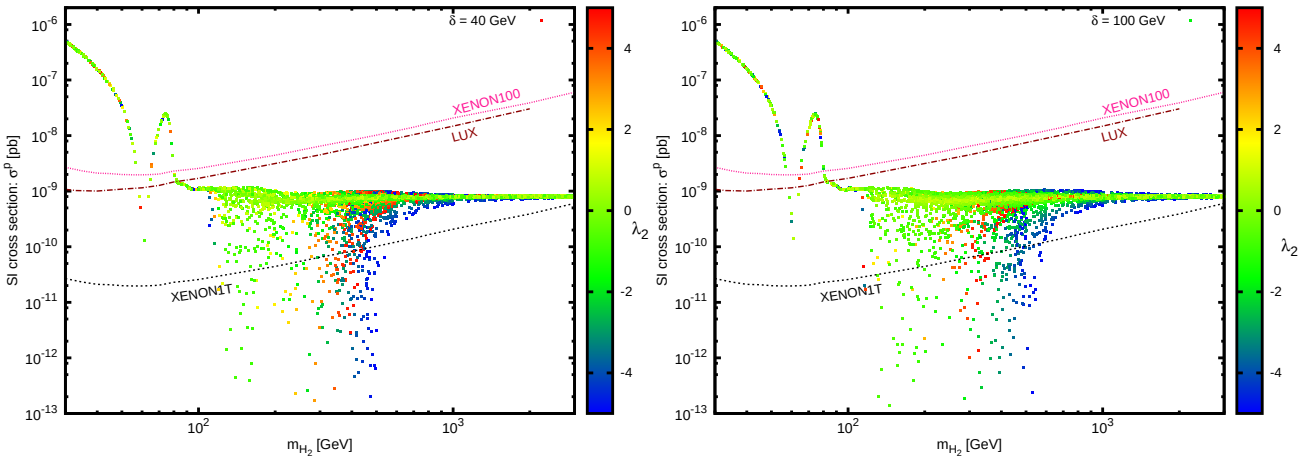

Figure 10: The same as in Fig. 7 with $-5 < \lambda_1 < 5$ and $-5 < \lambda_2 < 5$.

depicted in Fig. 10. Comparing our results in Figs. 9,10 with those in Figs. 6,7, we realize that the effects associated with the processes $H_2H_2 \to hhh$ and $H_2H_2 \to hhhh$ become sizable for $|\lambda_1| \gtrsim 1$ and $|\lambda_2| \gtrsim 1$.

For the current model, inelastic WIMP-nucleon interaction begins contributing for $\delta \sim$ KeV which is far smaller from the limits we have considered in this work i.e., $\delta \sim$ GeV.

6 Gamma-ray Emission from DM Annihilation

The analysis of Fermi Large Area Telescope (Fermi-LAT) data [70] (see [71] for the recent report) triggered by the authors in [72, 73] and continued by several groups [55, 56, 74–81] revealed an excess in the gamma-ray from the center of the Milky Way or Galaxy Center (GC), hence dubbed Galactic Center Excess (GCE). The

gamma-ray emission produced by the millisecond pulsars in the galaxy center can only contribute in 5-10% of the excess observed [82] [1]. Sources such as cosmic ray interactions are disfavored as well [83].

On the other hand, surprisingly the morphology and the spectrum of the GCE is well fitted when the dark matter annihilation into standard model particles is added in the background model used in the analyses. All diffuse background models where include the WIMP as a component agree in morphology. However, the position of the gamma-ray peak in the energy spectrum and the mass of the dark matter annihilating into SM particles varies by considering the systematic uncertainties in the background model [55, 56].

The dark matter candidate depending on its mass can annihilate into leptons, quarks, the gauge bosons and the Higgs boson. The gamma-ray is then produced through the cascade decays of these particles to neutral pion by the hadronization of the quarks, also through the bremsstrahlung of the charged gauge bosons and leptons. Among these processes the gamma-ray from the pion decay is dominated compared with the gamma emission from bremsstrahlung. The differential gamma-ray flux produced by a single W, Z, the Higgs boson and the top quark is depicted in Fig. 1 of [55]. It can be easily seen that the peak of the spectrum is moving towards the higher energies for heavier particles.

It was believed formerly (see e.g. [78,80]) that dark matter candidates with masses being only in the range of 30 GeV $< m_{\rm DM} <$ 50 GeV decaying into $\bar{b}b$ give an acceptable fit with the excess observed in the Fermi data. In the recent works however it is argued that taking into account the systematic uncertainties in the analysis of the Fermi data not only the mass range of dark matter for $b\bar{b}$ channel is enlarged into 35 GeV $< m_{\rm DM} <$ 165 GeV but also larger dark matter masses in annihilation to WW, ZZ, hh, and $t\bar{t}$ can be fitted well enough with the data [55]. Additionally, it is pointed out in [57] that DM mass up to about 74 GeV decaying into b quark pair and also DM annihilation into non-relativistic hh can fit well to the Fermi data.

We show that the gamma-ray excess in our scalar split model can be explained well. To this end, we obtain the photon flux produced by dark matter annihilation where the allowed values for the couplings are taken from the viable parameter space.

The gamma-ray flux is determined in terms of the annihilation cross section $\langle\sigma v\rangle_{\rm ann}$, the mass of the annihilating dark matter $m_{\rm DM}$, the gamma-ray spectrum generated per annihilation dN_γ/dE_γ and the density of dark matter ρ in the region of interest (ROI) is

$$\frac{d^2\Phi}{dE_\gamma d\Omega} = \frac{1}{16\pi}\frac{\langle\sigma v\rangle_{\rm ann}}{m_{\rm DM}^2}\frac{dN_\gamma}{dE_\gamma}\int_0^\infty dr\rho^2(r)\,, \tag{28}$$

The density of dark matter in the Milky Way galaxy is assumed to be spherically symmetric. The density distribution is then a function of r and is described by the generalized Navarro-Frenk-White (NFW) halo profile [84]:

$$\rho(r) = \rho_\odot(\frac{r_\odot}{r})^\gamma\Big(\frac{r_s+r_\odot}{r_s+r}\Big)^{3-\gamma}\,, \tag{29}$$

[1] Although a recent paper [85] associates GCE to the point-like sources such as millisecond pulsars.

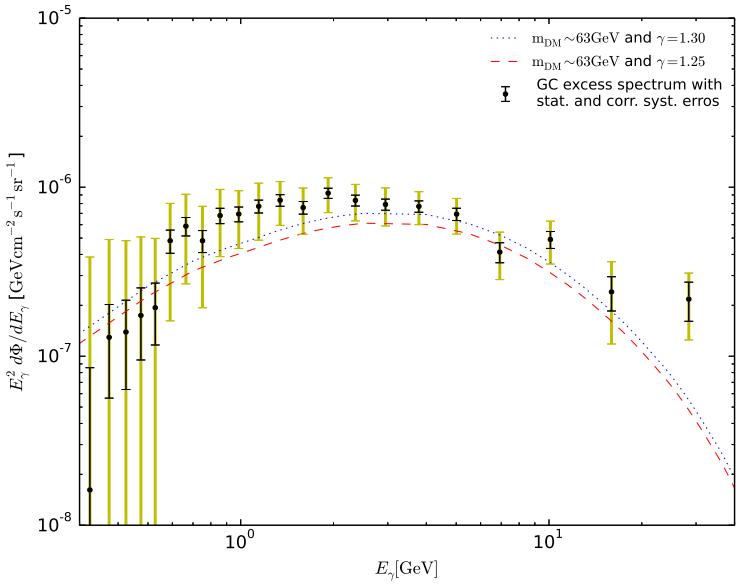

Figure 11: Shown is the gamma-ray flux multiplied by energy squared from annihilating dark matter computed in the scalar split WIMPs model for dark matter mass $m_{\rm DM} \sim 63$ GeV and $\delta = 100$ GeV. The black error bars accompanied with correlated systematic errors is the obtained flux from Fermi-LAT data [56].

where $r_s = 20$ kpc is the scale radius, $\rho_\odot = 0.3$ GeV/cm^3 is the local dark matter density at $r_\odot = 8.5$ kpc and r is the distance from the center of the galaxy to the point where the dark matter annihilation occurs. The parameter γ is the slope parameter being $\gamma = 1$ for the standard NFW. In our calculations we take γ within the interval $\gamma = 1.2 - 1.3$ used in the literature.

We find out that within the parameter space confined by relic density and direct detection in our DM model, there can be found regions producing gamma excess that are compatible with the fluxes provided by the Fermi data. We have used MicrOMEGAs package for computation of the gamma-ray flux in our particular model with dark matter mass $m_{\rm DM} \sim 63$ GeV, mass splitting $\delta = 100$ GeV, $\lambda_1 = 1.17 \times 10^{-2}$, $\lambda_2 = 6.07 \times 10^{-1}$ and $\sin\theta = 0.1$.

In Fig. 11 we present our results for the gamma-ray flux multiplied by the gamma energy squared for two slope parameters $\gamma = 1.25$ and $\gamma = 1.30$. In this figure it is shown the prediction of the scalar split WIMPs model for the gamma excess from annihilating dark matter of mass ~ 63 GeV with the total annihilation cross section $\langle\sigma\rangle_{\rm ann} \sim 4 \times 10^{-26}$cm^{3}s^{-1} and DM-nucleon elastic scattering cross section $\sigma_{\rm el} \sim 8 \times 10^{-10}$ pb, to be compared with the excess observed from the Fermi-LAT data. Comparison made with the data analysis provided by [56] at high Galactic latitudes $2^\circ \leq |b| \leq 20^\circ$ indicates the validity of the current model in explaining the Galactic gamma excess.

7 Conclusions

In this paper we have employed a simple model of dark matter called Scalar Split WIMPs with two scalars H_1 and H_2 interacting with SM particles through the Higgs portal. Depending on the mass splitting $\delta = m_{H_1} - m_{H_2}$ and the couplings in the model, the decay rate of the heavier scalar H_1 changes. For the parameter space explored in this work, the H_1 decay rate is much smaller than the age of the Universe. Therefore we have only one scalar H_2 that contributes in the DM relic abundance. The model possesses seven free parameters out of which only five parameters m_{H1}, m_{H_2}, λ_1, λ_2 and θ enter into the annihilation and co-annihilation cross section computations. The mass splitting parameter δ may change the viable parameter space in various computations.

We have examined our model with four observational and experimental bounds imposed by invisible Higgs decay, the amount of dark matter abundance, the limits put on DM-nucleon cross section by direct detection experiments, and the gamma excess found by the analyses on the Fermi-LAT data.

There is an important characteristic for the scalar split WIMP model that distinguishes that from the vastly studied singlet scalar models. In case we choose $-1 < \lambda_1 < 1$, $-1 < \lambda_2 < 1$, there can be found viable regions in the parameter space beyond the resonant region in the scalar split model with $m_{\rm DM}$ in the range around $57 - 200$ GeV for $\delta = 1$ GeV in Fig. 6 and around $125 - 200$ GeV for $\delta = 40, 100$ GeV in Figs. 7, which evade the future experiment bounds on the WIMP-nucleon elastic scattering cross section. The viable region is extended to higher DM mass up to ~ 1000 GeV if we choose $-5 < \lambda_1 < 5$, $-5 < \lambda_2 < 5$. For the DM candidates in the viable space that respect the XENON1T and LUX bounds, we have inferred that the presence of the co-annihilation (when the mass splitting is small) and the mixing effect in the scalar split model play a critical role in the new feature so that the model can evade easily the bounds from the future direct detection experiments.

This feature is absent in the singlet scalar model where as shown in [21] the viable region in the parameter space is confined in the resonant region with $m_{\rm DM}$ in the range $57 - 62$ GeV or for $m_{\rm DM} \gtrsim 4$ TeV by the forthcoming direct detection experiments.

We observe that changing the mass splitting δ has almost no effect on the invisible Higgs decay width. Furthermore, the behavior of the relic density for a wide range of dark matter mass has been studied when the mass splitting takes $\delta = 1, 4, 40, 100$ GeV. We observe that the relic density changes considerably by varying the mass splitting δ when $m_{\rm DM} \lesssim 60$ GeV or $m_{\rm DM} \gtrsim 400$ GeV.

In addition, the scalar split model predicts a gamma-ray excess for $m_{\rm DM} \sim 63$ GeV and $\delta = 100$ GeV which is in agreement in morphology and spectrum with the excess observed out of the Fermi-LAT data. To compute the gamma-ray flux which is produced by bremsstrahlung processes and the pion decay created from cascade annihilations of dark matter into SM final states, we have used the so-called generalized NFW halo profile for the dark matter density at high Galactic latitudes of the Milky Way galaxy.

A Annihilation Cross Sections

In this section we present the relevant annihilation cross section formula for Feynman diagrams with only two particles in the final state. The annihilation cross sections into fermion pairs for the dark matter candidate, H_2 is

$$\sigma_{\rm ann} v_{\rm rel}(H_2 H_2 \to \bar{f} f) = \frac{N_c m_f^2}{\pi}(1-\frac{4m_f^2}{s})^{\frac{3}{2}}\Big[\frac{(\lambda_1\cos^2\theta+\lambda_2\sin^2\theta-\lambda_{12}\sin\theta\cos\theta)^2}{(s-m_h^2)^2+m_h^2\Gamma_h^2}\Big], \quad (30)$$

and for annihilation into gauge bosons $W^\pm$ and Z is

$$\sigma_{\rm ann} v_{\rm rel}(H_2 H_2 \to \bar{W}^+W^-, ZZ) = \frac{1}{2\pi s}\Big[\frac{(\lambda_1\cos^2\theta+\lambda_2\sin^2\theta-\lambda_{12}\sin\theta\cos\theta)^2}{(s-m_h^2)^2+m_h^2\Gamma_h^2}\Big]\times$$
$$\Big[((s-2m_W^2)^2+8m_W^2)(1-\frac{4m_W^2}{s})^{\frac{1}{2}}+\frac{1}{2}((s-2m_Z^2)^2+8m_W^2)(1-\frac{4m_Z^2}{s})^{\frac{1}{2}}\Big]. \quad (31)$$

The annihilation cross section for the process $H_2H_2 \to hh$ involves three Feynman diagrams given in Fig. 2. The finall result reads

$$\sigma_{\rm ann} v_{\rm rel}(H_2 H_2 \to hh) = \frac{\sqrt{1-4m_h^2/s}}{32\pi^2 s}\int d\Omega\Big[2\beta^2+\frac{72v^4\beta^2\lambda_H^2}{(s-m_h^2)^2}+\frac{v^4\alpha^4}{(t-m_{H_1}^2)^2}$$
$$+\frac{v^4\alpha^4}{(u-m_{H_1}^2)^2}+\frac{16v^4\beta^4}{(t-m_{H_2}^2)^2}+\frac{16v^4\beta^4}{(u-m_{H_2}^2)^2}+\frac{16v^2\beta^3}{t-m_{H_2}^2}+\frac{16v^2\beta^3}{u-m_{H_2}^2}+\frac{4v^2\beta\alpha^2}{t-m_{H_1}^2}$$
$$+\frac{4v^2\beta\alpha^2}{u-m_{H_1}^2}-\frac{24v^2\beta^2\lambda_H}{s-m_h^2}-\frac{96v^4\beta^3\lambda_H}{(s-m_h^2)(t-m_{H_2}^2)}-\frac{96v^4\beta^3\lambda_H}{(s-m_h^2)(u-m_{H_2}^2)}-\frac{24v^4\beta\alpha^2\lambda_H}{(s-m_h^2)(t-m_{H_1}^2)}$$
$$-\frac{24v^4\beta\alpha^2\lambda_H}{(s-m_h^2)(u-m_{H_1}^2)}+\frac{16v^4\beta^4}{(t-m_{H_2}^2)(u-m_{H_2}^2)}+\frac{v^4\alpha^4}{(t-m_{H_1}^2)(u-m_{H_1}^2)}+\frac{8v^4\alpha^2\beta^2}{(t-m_{H_1}^2)(t-m_{H_2}^2)}$$
$$+\frac{8v^4\alpha^2\beta^2}{(t-m_{H_1}^2)(u-m_{H_2}^2)}+\frac{8v^4\alpha^2\beta^2}{(u-m_{H_1}^2)(t-m_{H_2}^2)}+\frac{8v^4\alpha^2\beta^2}{(u-m_{H_1}^2)(u-m_{H_2}^2)}\Big], \quad (32)$$

where $\alpha = (\lambda_1-\lambda_2)\sin 2\theta + \lambda_{12}\cos 2\theta$ and $\beta = \lambda_1\cos^2\theta+\lambda_2\sin^2\theta-\lambda_{12}\sin\theta\cos\theta$. In the process $H_2(p_1)\ H_2(p_2) \to h(p_3)\ h(p_4)$, the Mandelstam variables are $s = (p_1+p_2)^2$, $t=(p_1-p_3)^2$ and $u=(p_1-p_4)^2$.

References

[1] P. A. R. Ade *et al.* [Planck Collaboration], Astron. Astrophys. **571** (2014) A16 [arXiv:1303.5076 [astro-ph.CO]].

[2] G. Hinshaw *et al.* [WMAP Collaboration], Astrophys. J. Suppl. **208** (2013) 19 [arXiv:1212.5226 [astro-ph.CO]].

[3] G. Bertone, D. Hooper and J. Silk, Phys. Rept. **405** (2005) 279 [hep-ph/0404175].

[4] L. Bergstrom, Rept. Prog. Phys. **63** (2000) 793 [hep-ph/0002126].

[5] C. P. Burgess, M. Pospelov and T. ter Veldhuis, Nucl. Phys. B **619** (2001) 709 [hep-ph/0011335].

[6] J. McDonald, Phys. Rev. D **50** (1994) 3637 [hep-ph/0702143 [HEP-PH]].

[7] M. Cirelli, N. Fornengo and A. Strumia, Nucl. Phys. B **753** (2006) 178 [hep-ph/0512090].

[8] M. Pospelov and A. Ritz, Phys. Rev. D **84** (2011) 113001 [arXiv:1109.4872 [hep-ph]].

[9] L. Lopez-Honorez, T. Schwetz and J. Zupan, Phys. Lett. B **716** (2012) 179 [arXiv:1203.2064 [hep-ph]].

[10] V. Barger, P. Langacker, M. McCaskey, M. Ramsey-Musolf and G. Shaughnessy, Phys. Rev. D **79** (2009) 015018 [arXiv:0811.0393 [hep-ph]].

[11] M. Pospelov, A. Ritz and M. B. Voloshin, Phys. Lett. B **662** (2008) 53 [arXiv:0711.4866 [hep-ph]].

[12] M. R. Buckley, D. Feld and D. Goncalves, arXiv:1410.6497 [hep-ph].

[13] D. S. Akerib *et al.* [LUX Collaboration], Phys. Rev. Lett. **112** (2014) 091303 [arXiv:1310.8214 [astro-ph.CO]].

[14] E. Aprile *et al.* [XENON100 Collaboration], Phys. Rev. Lett. **109** (2012) 181301 [arXiv:1207.5988 [astro-ph.CO]].

[15] M. Beltran, D. Hooper, E. W. Kolb, Z. A. C. Krusberg and T. M. P. Tait, JHEP **1009** (2010) 037 [arXiv:1002.4137 [hep-ph]].

[16] J. Goodman, M. Ibe, A. Rajaraman, W. Shepherd, T. M. P. Tait and H. B. Yu, Phys. Rev. D **82** (2010) 116010 [arXiv:1008.1783 [hep-ph]].

[17] Y. Bai, P. J. Fox and R. Harnik, JHEP **1012** (2010) 048 [arXiv:1005.3797 [hep-ph]].

[18] G. Belanger, B. Dumont, U. Ellwanger, J. F. Gunion and S. Kraml, Phys. Lett. B **723** (2013) 340 [arXiv:1302.5694 [hep-ph]].

[19] N. Arkani-Hamed, A. G. Cohen, T. Gregoire and J. G. Wacker, JHEP **0208** (2002) 020 [hep-ph/0202089].

[20] V. Barger, P. Langacker, M. McCaskey, M. J. Ramsey-Musolf and G. Shaughnessy, Phys. Rev. D **77** (2008) 035005 [arXiv:0706.4311 [hep-ph]].

[21] J. M. Cline, K. Kainulainen, P. Scott and C. Weniger, Phys. Rev. D **88** (2013) 055025 [arXiv:1306.4710 [hep-ph]].

[22] C. Boehm, M. J. Dolan, C. McCabe, M. Spannowsky and C. J. Wallace, JCAP **1405** (2014) 009 [arXiv:1401.6458 [hep-ph]].

[23] A. Berlin, D. Hooper and S. D. McDermott, Phys. Rev. D **89** (2014) 115022 [arXiv:1404.0022 [hep-ph]].

[24] C. Boehm, M. J. Dolan and C. McCabe, Phys. Rev. D **90** (2014) 023531 [arXiv:1404.4977 [hep-ph]].

[25] P. Ko, W. I. Park and Y. Tang, JCAP **1409** (2014) 013 [arXiv:1404.5257 [hep-ph]].

[26] M. Abdullah, A. DiFranzo, A. Rajaraman, T. M. P. Tait, P. Tanedo and A. M. Wijangco, Phys. Rev. D **90** (2014) 3, 035004 [arXiv:1404.6528 [hep-ph]].

[27] A. Berlin, P. Gratia, D. Hooper and S. D. McDermott, Phys. Rev. D **90** (2014) 015032 [arXiv:1405.5204 [hep-ph]].

[28] J. M. Cline, G. Dupuis, Z. Liu and W. Xue, JHEP **1408** (2014) 131 [arXiv:1405.7691 [hep-ph]].

[29] L. Wang, arXiv:1406.3598 [hep-ph].

[30] C. Cheung, M. Papucci, D. Sanford, N. R. Shah and K. M. Zurek, Phys. Rev. D **90** (2014) 075011 [arXiv:1406.6372 [hep-ph]].

[31] C. Balzs and T. Li, Phys. Rev. D **90** (2014) 055026 [arXiv:1407.0174 [hep-ph]].

[32] J. Huang, T. Liu, L. T. Wang and F. Yu, Phys. Rev. D **90** (2014) 115006 [arXiv:1407.0038 [hep-ph]].

[33] K. Ghorbani, JCAP **1501** (2015) 015 [arXiv:1408.4929 [hep-ph]].

[34] A. D. Banik and D. Majumdar, arXiv:1408.5795 [hep-ph].

[35] D. Borah and A. Dasgupta, arXiv:1409.1406 [hep-ph].

[36] M. Cahill-Rowley, J. Gainer, J. Hewett and T. Rizzo, arXiv:1409.1573 [hep-ph].

[37] J. Guo, J. Li, T. Li and A. G. Williams, arXiv:1409.7864 [hep-ph].

[38] M. J. Dolan, C. McCabe, F. Kahlhoefer and K. Schmidt-Hoberg, arXiv:1412.5174 [hep-ph].

[39] A. Biswas, arXiv:1412.1663 [hep-ph].

[40] K. P. Modak, D. Majumdar and S. Rakshit, JCAP **1503** (2015) 011 [arXiv:1312.7488 [hep-ph]].

[41] J. Cao, L. Shang, P. Wu, J. M. Yang and Y. Zhang, arXiv:1410.3239 [hep-ph].

[42] N. F. Bell, S. Horiuchi and I. M. Shoemaker, Phys. Rev. D **91** (2015) 023505 [arXiv:1408.5142 [hep-ph]].

[43] W. Detmold, M. McCullough and A. Pochinsky, Phys. Rev. D **90** (2014) 11, 115013 [arXiv:1406.2276 [hep-ph]].

[44] K. Cheung, W. C. Huang and Y. L. S. Tsai, arXiv:1411.2619 [hep-ph].

[45] P. Ko and Y. Tang, JCAP **1501** (2015) 023 [arXiv:1407.5492 [hep-ph]].

[46] J. D. Ruiz-Alvarez, C. A. de S.Pires, F. S. Queiroz, D. Restrepo and P. S. Rodrigues da Silva, Phys. Rev. D **86** (2012) 075011 [arXiv:1206.5779 [hep-ph]].

[47] T. Basak and T. Mondal, arXiv:1405.4877 [hep-ph].

[48] A. Martin, J. Shelton and J. Unwin, Phys. Rev. D **90** (2014) 10, 103513 [arXiv:1405.0272 [hep-ph]].

[49] E. Hardy, R. Lasenby and J. Unwin, JHEP **1407** (2014) 049 [arXiv:1402.4500 [hep-ph]].

[50] G. Marshall and R. Primulando, JHEP **1105** (2011) 026 [arXiv:1102.0492 [hep-ph]].

[51] N. Okada and O. Seto, Phys. Rev. D **89** (2014) 043525 [arXiv:1310.5991 [hep-ph]].

[52] J. Liu, N. Weiner and W. Xue, arXiv:1412.1485 [hep-ph].

[53] M. Freytsis, D. J. Robinson and Y. Tsai, arXiv:1410.3818 [hep-ph].

[54] T. Lacroix, C. Boehm and J. Silk, Phys. Rev. D **90** (2014) 4, 043508 [arXiv:1403.1987 [astro-ph.HE]].

[55] P. Agrawal, B. Batell, P. J. Fox and R. Harnik, arXiv:1411.2592 [hep-ph].

[56] F. Calore, I. Cholis and C. Weniger, arXiv:1409.0042 [astro-ph.CO].

[57] F. Calore, I. Cholis, C. McCabe and C. Weniger, arXiv:1411.4647 [hep-ph].

[58] K. Griest and D. Seckel, Phys. Rev. D **43** (1991) 3191. doi:10.1103/PhysRevD.43.3191

[59] J. Edsjo and P. Gondolo, Phys. Rev. D **56** (1997) 1879 doi:10.1103/PhysRevD.56.1879 [hep-ph/9704361].

[60] G. Belanger, F. Boudjema, A. Pukhov and A. Semenov, Comput. Phys. Commun. **174** (2006) 577 doi:10.1016/j.cpc.2005.12.005 [hep-ph/0405253].

[61] A. Belyaev, N. D. Christensen and A. Pukhov, Comput. Phys. Commun. **184** (2013) 1729 [arXiv:1207.6082 [hep-ph]].

[62] A. Semenov, arXiv:1005.1909 [hep-ph].

[63] G. Belanger, F. Boudjema, A. Pukhov and A. Semenov, Comput. Phys. Commun. **185** (2014) 960 [arXiv:1305.0237 [hep-ph]].

[64] S. Heinemeyer *et al.* [LHC Higgs Cross Section Working Group Collaboration], arXiv:1307.1347 [hep-ph].

[65] J. R. Ellis, K. A. Olive and C. Savage, Phys. Rev. D **77** (2008) 065026 [arXiv:0801.3656 [hep-ph]].

[66] G. Belanger, F. Boudjema, A. Pukhov and A. Semenov, Comput. Phys. Commun. **180** (2009) 747 [arXiv:0803.2360 [hep-ph]].

[67] T. Nihei and M. Sasagawa, Phys. Rev. D **70** (2004) 055011 [Erratum-ibid. D **70** (2004) 079901] [hep-ph/0404100].

[68] J. R. Ellis, A. Ferstl and K. A. Olive, Phys. Lett. B **481** (2000) 304 [hep-ph/0001005].

[69] A. Crivellin, M. Hoferichter and M. Procura, Phys. Rev. D **89** (2014) 054021 [arXiv:1312.4951 [hep-ph]].

[70] R. Rando [Fermi LAT Collaboration], arXiv:0907.0626 [astro-ph.IM].

[71] Fermi-LAT Collaboration, S. Murgia, "Observation of the High Energy Gamma-ray Emission Towards the Galactic Center". http://fermi.gsfc.nasa.gov/science/mtgs/symposia/2014/program/08-Murgia.pdf, (October 2014).

[72] L. Goodenough and D. Hooper, arXiv:0910.2998 [hep-ph].

[73] D. Hooper and L. Goodenough, Phys. Lett. B **697** (2011) 412 [arXiv:1010.2752 [hep-ph]].

[74] A. Boyarsky, D. Malyshev and O. Ruchayskiy, Phys. Lett. B **705** (2011) 165 [arXiv:1012.5839 [hep-ph]].

[75] D. Hooper and T. Linden, Phys. Rev. D **84** (2011) 123005 [arXiv:1110.0006 [astro-ph.HE]].

[76] K. N. Abazajian and M. Kaplinghat, Phys. Rev. D **86** (2012) 083511 [arXiv:1207.6047 [astro-ph.HE]].

[77] D. Hooper and T. R. Slatyer, Phys. Dark Univ. **2** (2013) 118 [arXiv:1302.6589 [astro-ph.HE]].

[78] C. Gordon and O. Macias, Phys. Rev. D **88** (2013) 083521 [Erratum-ibid. D **89** (2014) 4, 049901] [arXiv:1306.5725 [astro-ph.HE]].

[79] K. N. Abazajian, N. Canac, S. Horiuchi and M. Kaplinghat, Phys. Rev. D **90** (2014) 023526 [arXiv:1402.4090 [astro-ph.HE]].

[80] T. Daylan, D. P. Finkbeiner, D. Hooper, T. Linden, S. K. N. Portillo, N. L. Rodd and T. R. Slatyer, arXiv:1402.6703 [astro-ph.HE].

[81] B. Zhou, Y. F. Liang, X. Huang, X. Li, Y. Z. Fan, L. Feng and J. Chang, arXiv:1406.6948 [astro-ph.HE].

[82] D. Hooper, I. Cholis, T. Linden, J. Siegal-Gaskins and T. Slatyer, Phys. Rev. D **88** (2013) 083009 [arXiv:1305.0830 [astro-ph.HE]].

[83] T. Linden, E. Lovegrove and S. Profumo, Astrophys. J. **753** (2012) 41 [arXiv:1203.3539 [astro-ph.HE]].

[84] J. F. Navarro, C. S. Frenk and S. D. M. White, Astrophys. J. **462** (1996) 563 [astro-ph/9508025].

[85] R. Bartels, S. Krishnamurthy and C. Weniger, arXiv:1506.05104 [astro-ph.HE].